Electronic Supplementary Material (ESI) for Soft Matter.

Supplemental information for: Directional-dependent pockets drive columnar–columnar coexistence

Álvaro González García,[*,†] Remco Tuinier,[*,†] Gijsbertus de With,[¶] and Alejandro Cuetos[§]

† *Van 't Hoff Laboratory for Physical and Colloid Chemistry, Department of Chemistry & Debye Institute, Utrecht University, The Netherlands*

‡ *Laboratory of Physical Chemistry, Department of Chemical Engineering and Chemistry & Institue for Complex Molecular Systems (ICMS), Eindhoven University of Technology, Eindhoven, The Netherlands*

¶ *Laboratory of Physical Chemistry, Department of Chemical Engineering and Chemistry, Eindhoven University of Technology, The Netherlands*

§ *Department of Physical, Chemical and Natural Systems, Universidad Pablo Olavide, 41013 Sevilla, Spain*

E-mail: a.gonzalez.garcia@tue.nl; r.tuinier@tue.nl

Free Volume theory

We use free volume theory (FVT) to calculate the thermodynamics of the discotic-depletant mixtures at hand. FVT follows a semi-grand canonical approach where depletion effects on the discotic–depletant system of interest (S) are assessed by fixing the depletant volume fraction in a reservoir (R) where only depletants are present, $\phi_{\rm d}^{\rm R}$. This reservoir corresponds to the depletant bulk solution. Three main ingredients are required to calculate thermodynamic properties of platelet–depletant mixtures via free volume theory (FVT): (1) the pure platelet Helmholtz energies of the different phases F_k,[1] (2) the excluded volume between discotics and depletants[2] $v_{\rm exc}^{\rm p-s}$, and (3) the free volume available for depletants in the different phases α_k. The index k runs over the possible phase states of the systems, namely isotropic (I), nematic (N) and columnar (C). This theory accounts for partitioning of depletants over the different phases.[3] However, it has been shown recently that a better account of the partitioning of (tiny) depletants over dense phases brings FVT closer to more evolved theories, simulations and experimental results.[4] Here, we consider the directionality of the depletion patches between discotics on geometrical grounds. For ideal depletants (penetrable hard spheres, PHSs), the grand-potential Ω of the system reads:

$$\frac{\beta\Omega v_{\rm c}}{V} \equiv \widetilde{\Omega}_k = \widetilde{F}_k - \widetilde{\Pi}_{\rm d}^{\rm R}\alpha_k\frac{v_{\rm c}}{v_{\rm d}} \ , \tag{S1}$$

where Ω is the normalized grand potential, $\widetilde{F}_k \equiv \beta F_k v_{\rm c}/V$ is the normalized Helmholtz free energy of the depletant-free phase-state k and $\beta\Pi_{\rm d}^{\rm R}v_{\rm d} \equiv \widetilde{\Pi}_{\rm d}^{\rm R} = \phi_{\rm d}^{\rm R}$ is the osmotic pressure of depletants in R. Here, $\beta \equiv 1/(k_{\rm B}T)$ with $k_{\rm B}$ the Boltzmann constant and T the absolute temperature.

From this $\widetilde{\Omega}$, the (normalized) chemical potential $\widetilde{\mu}_k$ of the discs and the osmotic pressure $\widetilde{\Pi}_k$ of the particle–depletant mixture of interest follow as:

$$\beta\mu_k \equiv \widetilde{\mu}_k = \left(\frac{\partial\widetilde{\Omega}_k}{\partial\phi_{\rm c}}\right)_{T,V,N_{\rm d}^R} \ ; \ \beta\Pi_k v_{\rm c} \equiv \widetilde{\Pi}_k = \phi_{\rm c}\widetilde{\mu}_k - \widetilde{\Omega}_k \ , \tag{S2}$$

with $N_{\rm d}^{\rm R}$ the number of depletants in R. Using these quantities, phase coexistences follow from:

$$\widetilde{\mu}_i = \widetilde{\mu}_j = ..., \text{ and } \widetilde{\Pi}_i = \widetilde{\Pi}_j = ... \ , \tag{S3}$$

where i and j denote the two (or more) coexisting phases of kind i, j. Whenever a phase state has a critical point (CP), there is an isostructural phase coexistence, which can be stable or metastable. The transition from a potentially stable to a metastable isostructural phase coexistence is defined by the critical end point (CEP), where the CP and the triple or quadruple point of the corresponding coexistences merge.[5,6] The system volume fraction of depletants in the columnar phase is given as $\phi_{\rm d}^{\rm S} = \alpha_{\rm C}\phi_{\rm d}^{\rm R}$, and in the two distinctive directions it follows that $\phi_{\rm d}^{\rm S,\parallel} = \alpha_{\rm C}^{\parallel}\phi_{\rm d}^{\rm R}$, and $\phi_{\rm d}^{\rm S,\perp} = \alpha_{\rm C}^{\perp}\phi_{\rm d}^{\rm R}$. In this SI, the distinction between S and R is clearly indicated for the depletants. In the isotropic and nematic state, $\phi_{\rm d}^{\rm S} = \alpha_{\rm I}\phi_{\rm d}^{\rm R}$ and $\phi_{\rm d}^{\rm S} = \alpha_{\rm N}\phi_{\rm d}^{\rm R}$. Note that the free volume fraction for depletants in both the isotropic and nematic phases is calculated following a SPT approach as was done in the original FVT.

The only remaining unknown parameter in Equation S1 is the free volume fraction for depletants in the system on a k-phase, α_k. Different approaches can be followed, which are discussed in the next subsections.

Free volume fraction from SPT

Commonly, α is calculated by using a Scaled Particle Theory (SPT) approach,[2] as done in original FVT[7] which focused on more dilute systems consisting of spherical colloidal particles. Widom's insertion theorem[8] relates the free volume fraction α to the work ω required to bring a depletant from R to S via:

$$\alpha = \frac{\langle V_{\rm free}\rangle_{\rm o}}{V} = e^{-\beta\omega}, \tag{S4}$$

where $\langle V_{\rm free}\rangle_{\rm o}$ is the average free volume for depletants in the undistorted (depletant-free) system. This work, ω, is approximated using Scaled Particle Theory (SPT),[9,10] by connecting

the limits of inserting a very small depletant and a very big depletant in the system of interest, followed by scaling back to the actual size of the depletant. We only consider spherical depletants. Hence, a single scaling factor (Λ) enables to express this work by combining the limiting results for $\Lambda \to 0$ and $\Lambda \to \infty$:

$$\omega(\Lambda) = \underbrace{\omega(0) + \left.\frac{\partial \omega}{\partial \Lambda}\right|_{\Lambda=0} \Lambda + \frac{1}{2} \left.\frac{\partial^2 \omega}{\partial \Lambda^2}\right|_{\Lambda=0} \Lambda^2}_{\Lambda \ll 1} + \underbrace{v_{\mathrm{d}} \Pi_k^{\mathrm{o}}}_{\Lambda \gg 1} \ , \tag{S5}$$

where Π_k^{o} is the osmotic pressure of the depletant-free system (in a phase k). In the small depletant insertion limit ($\Lambda \ll 1$) there is no overlap of depletion zones: $\alpha \to [1 - \phi_{\mathrm{c}} v_{\mathrm{exc}}^{\text{HC-PHS}}(\Lambda)/v_{\mathrm{c}}]$, with $v_{\mathrm{exc}}^{\text{HC-PHS}}$ the excluded volume between a hard cylinder and a penetrable hard sphere (PHS):

$$v_{\mathrm{exc}}^{\text{HC-PHS}} = \frac{\pi}{2} D^2 \delta + \frac{\pi}{3} L \left(D + 2\delta\right)^2 + \frac{\pi^2}{2} \delta^2 \left(D + \frac{8\delta}{3\pi}\right) \ . \tag{S6}$$

Equation S4 then allows writing $\omega(\Lambda \ll 1)$ as:

$$\beta\omega(\Lambda \ll 1) = -\ln\left[1 - \phi_{\mathrm{c}} \left(\frac{v_{\mathrm{exc}}^{\text{HC-PHS}}(\Lambda)}{v_{\mathrm{c}}}\right)\right] , \tag{S7}$$

where the scaled depletion volume is obtained by scaling the depletant size: $\delta \to \Lambda\delta$. For big depletants ($\Lambda \to \infty$) we assume that the insertion work ω is the work required to create a cavity with the size of the depletant in the system. We use normalised units also in the big-depletant limit for convenience, thus:

$$\beta\omega(\Lambda \gg 1) = \frac{v_{\mathrm{d}}(\Lambda)}{v_{\mathrm{c}}} \widetilde{\Pi}_k^{\mathrm{o}} \ . \tag{S8}$$

Inserting Equation S7 and S8 into Equation S4 yields, after some algebra, the following expression for α_k^{SPT}, where $k = \{\mathrm{I}, \mathrm{N}, \mathrm{C}\}$

$$\alpha_k^{\mathrm{SPT}} = (1 - \phi_{\mathrm{c}}) \exp\left[-Q_{\mathrm{s}}\right] \exp\left[-\frac{v_{\mathrm{d}}}{v_{\mathrm{c}}} \widetilde{\Pi}_{\mathrm{k}}^{\mathrm{o}}\right] , \tag{S9}$$

where the shape parameter Q_{s} reads:

$$Q_{\mathrm{s}} = q\left(\frac{1}{\Lambda} + \frac{\pi q}{2\Lambda} + q + 2\right) y(\phi_{\mathrm{c}}) + 2q^2 \left(\frac{1}{4\Lambda^2} + \frac{1}{\Lambda} + 1\right) y(\phi_{\mathrm{c}})^2 , \tag{S10}$$

which includes the auxiliary function

$$y(\phi_{\mathrm{c}}) = \frac{\phi_{\mathrm{c}}}{1 - \phi_{\mathrm{c}}} . \tag{S11}$$

We employ the SPT-derived αs for the isotropic and nematic phases of depletant–discotic mixtures. Note here that, according to the original FVT, all information on the free volume available is accounted for only in the terms of the depletant-free osmotic pressure. Although this is accurate for large depletants, for tiny depletants that fit in the specific pockets of the dense liquid-crystalline phase state considered the SPT-derived α underestimates the free volume available for depletants in the system.[4]

Geometrical free volume fractions

Alternatively to the SPT-derived free volume fraction for depletants α commonly used in FVT, a geometrical approach is followed here to calculate α in the columnar phase. We follow the ideas put forward in[4] to calculate a geometrical free volume fraction for PHS in a columnar state. Let V_{UC} be the volume of the columnar unit cell, such that:

$$V_{\mathrm{UC}} = \frac{3\pi^2 v_{\mathrm{c}}}{16\phi_{\mathrm{c}}} . \tag{S12}$$

The free volume for depletants is simply the volume unoccupied by the depletion zones if there is no overlap of depletion zones (discotic volume fractions far from the close packing). As mentioned in the main text, overlap of the depletion zones leads to an increase of the free volume fraction for depletants. In the case of the hard cylinders (HCs), overlap of the depletion zones occurs either from the side or from the flat phases of the hard platelet. These two contributions are split. One must account for the total number of overlaps, which corresponds to the effective number of small systems: nine in the intercolumnar direction and three in the intracolumnar one. This allows to express $\alpha_{\mathrm{C}}^{\mathrm{geo}}$ in a generic form:

$$\alpha_{\mathrm{C}} = \begin{cases} 1 - \dfrac{3v_{\mathrm{excl}}^{\text{HC-PHS}}}{V_{\mathrm{UC}}} & \text{if } \phi_{\mathrm{c}} < \phi_{\mathrm{c}}^{\parallel} \text{ (no overlap)}, \\ 1 - \left(\dfrac{3v_{\mathrm{excl}}^{\text{HC-PHS}}}{V_{\mathrm{UC}}} - \dfrac{3v_{\mathrm{overl}}^{\parallel}}{V_{\mathrm{UC}}} \right) & \text{if } \phi_{\mathrm{c}}^{\parallel} \leq \phi_{\mathrm{c}} < \phi_{\mathrm{c}}^{\perp} \text{ (overlap in } r_{\parallel}) \\ 1 - \left(\dfrac{3v_{\mathrm{excl}}^{\text{HC-PHS}}}{V_{\mathrm{UC}}} - \dfrac{3v_{\mathrm{overl}}^{\parallel}}{V_{\mathrm{UC}}} - \dfrac{9v_{\mathrm{overl}}^{\perp}}{V_{\mathrm{UC}}} \right) & \text{if } \phi_{\mathrm{c}} \geq \phi_{\mathrm{c}}^{\perp} \text{ (overlap in } r_{\parallel} \text{ and } r_{\perp}), \end{cases} \tag{S13}$$

where $\phi_{\mathrm{c}}^{\parallel}$ is the solution of the equation

$$\widehat{\Delta}_{\parallel}(\phi_{\mathrm{c}}) = 1 + q/\Lambda \ , \tag{S14}$$

and $\phi_{\mathrm{c}}^{\perp}$ follows from solving

$$\widehat{\Delta}_{\perp}(\phi_{\mathrm{c}}) = 1 + q. \tag{S15}$$

The term $v_{\mathrm{excl}}^{\text{HC-PHS}}$ in Equation S13 accounts for the depletion zone volume. Also note that with the approach described here we only account for two-body overlaps of the depletion zones, which is sufficient for sufficiently small q-values. However, the geometrical approach is expected to fail in case of large q-values, at which the SPT method becomes more realistic as it accounts for multiple overlap of depletion zones. Further, in Equation S13 the condition 'no free volume for depletants' is not shown for simplicity. Upon some algebra, these three

different contributions read:

$$\begin{aligned}
\frac{3v_{\text{excl}}^{\text{HP-PHS}}}{V_{\text{UC}}} &= \phi_{\text{c}}\left[(1+q)^2+\frac{q}{6\Lambda}\left(6+3\pi q+4q^2\right)\right] \\
\frac{3v_{\text{overl}}^{\parallel}}{V_{\text{UC}}} &= \phi_{\text{c}}\left(1+\frac{q}{\Lambda}\right)-\frac{\pi}{2\sqrt{3}\widehat{\Delta}_{\perp}^2}+\frac{2\phi_{\text{c}}}{3}\left[3\Lambda A_2(q/(2\Lambda),\widehat{\Delta}_{\parallel}-1)+\Lambda^2\left(\widehat{\Delta}_{\parallel}-1\right)^3+\frac{q^3}{\Lambda}\right] \\
\frac{9v_{\text{overl}}^{\perp}}{V_{\text{UC}}} &= \frac{\phi_{\text{c}}}{\pi}12A_2\left(\frac{1+q}{2},\widehat{\Delta}_{\perp}\right),
\end{aligned} \tag{S16}$$

where A_2 is the overlap area between two discs with radius R at a separation distance r:

$$A_2(R,r)=2R^2\cos^{-1}\left(\frac{r}{2R}\right)-\frac{1}{2}r\sqrt{4R^2-r^2} \tag{S17}$$

We finally note that the algebraic complexity of Equation S13 arises mostly due to the contribution of the depletion zone near the edges of the platelet. A simpler, yet slightly less accurate expression for α_{C} arises if one does not consider the contribution to the depletion zones near the edges of the platelets. The functional form of $\alpha_{\text{C}}^{\text{simp}}$ is similar to in Equation S13, but with simpler versions of the $v_{\text{excl}}^{\text{HP-PHS}}$ and $v_{\text{overl}}^{\parallel}$:

$$\begin{aligned}
\frac{3v_{\text{excl}}^{\text{HP-PHS}}}{V_{\text{UC}}} &= \phi_{\text{c}}[(1+q)^2+q/\Lambda] \\
\frac{3v_{\text{overl}}^{\parallel}}{V_{\text{UC}}} &= \phi_{\text{c}}\left(1+\frac{q}{\Lambda}\right)-\frac{\pi}{2\sqrt{3}\widetilde{\Delta}_{\perp}^2}\ .
\end{aligned} \tag{S18}$$

The three predictions for the free volume fraction for depletants in the columnar phase are compared in Figure S1. In order to quantify the number of depletants in the inter- and intra-columnar directions, directional αs must be defined in $r_{\perp}$ and $r_{\parallel}$. Analysis of the two different effective small systems present leads to the following expressions:

$$\alpha_{\text{C}}^{\parallel}=\begin{cases}1-\dfrac{q/\Lambda+1}{\widehat{\Delta}_{\parallel}}, & \text{if } \phi_{\text{c}}<\phi_{\text{c}}^{\parallel} \text{ (no overlap in } r_{\parallel}\text{)}, \\ 0 & \text{if } \phi_{\text{c}}>\phi_{\text{c}}^{\parallel} \text{ (overlap in } r_{\parallel}\text{)}\ ,\end{cases} \tag{S19}$$

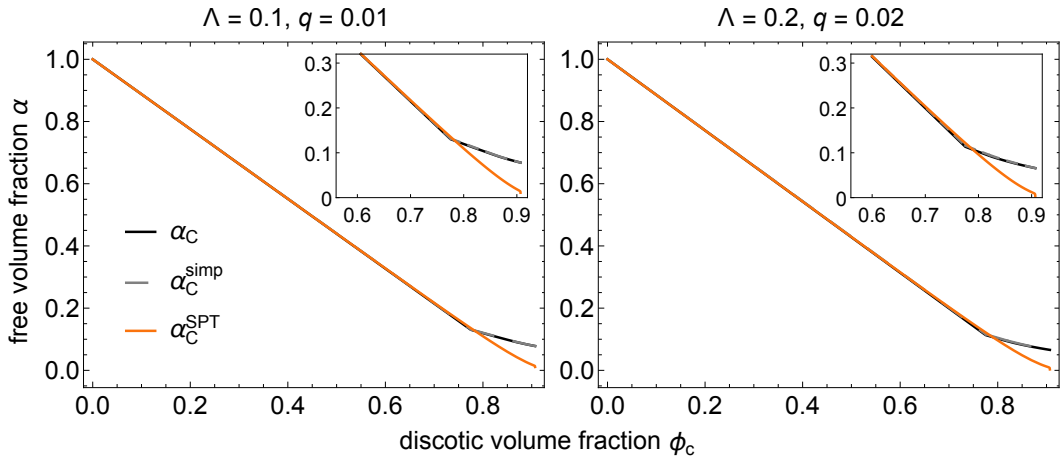

Figure S1: Free volume fraction for depletants in a columnar state as a function of the discotic volume fraction considering Equation S13, its simplified version (see main text), and the SPT approach for the system parameters $\{\Lambda, q\}$ indicated. Insets zoom in on high discotic volume fractions. The dashed grey curved corresponding to the simplified α_{C} expression practically overlaps with the more accurate one.

and

$$\alpha_{\mathrm{C}}^{\perp} = \begin{cases} 1-(1+q)^2\phi_{\mathrm{c}}, & \text{if } \phi_{\mathrm{c}} < \phi_{\mathrm{c}}^{\perp} \text{ (no overlap in } r_{\perp}), \\ 1-\left[(1+q)^2\phi_{\mathrm{c}} - \dfrac{3\phi_{\mathrm{c}}A_2(q+1,2\widehat{\Delta}\perp)}{\pi}\right] & \text{if } \phi_{\mathrm{c}} > \phi_{\mathrm{c}}^{\perp} \text{ (overlap in } r_{\perp}) \ . \end{cases} \tag{S20}$$

From the comparisons in Figure S1, it follows that the geometrical (α_{C}) and the SPT-derived $\alpha_{\mathrm{C}}^{\mathrm{SPT}}$ expressions match up to the discotic volume fraction $\phi_{\mathrm{c}}^{\parallel}$ at which overlap of the depletion zones in $r_{\parallel}$ occurs. Furthermore, considering a simplified geometrical α_{C} or the complete expression has a barely perceptible effect due to the tiny size of the depletants considered (see also insets in the middle panels in Figures S6 to S9). It is also clear from the middle panels in Figures S6 to S9, that the weighted average mean (WAM) of the orientation-dependent α_{C} is close to the complete expression used.

Simulations

Two different simulation procedures are followed: (1) direct coexistence simulations, and (2) characterization of the equilibrium configurations. In both cases, platelets are considered as hard oblate spherocylinders (OHSCs)[11] mixed with a non-adsorbing species (depletants) modelled as penetrable hard spheres (PHSs). Direct discotic–discotic and depletant–discotic interactions are hard, whereas the depletant–depletant interactions are ideal, so ghost-like.

Via the direct coexistence simulations we confirm the C_1–C_2 coexistence. These simulations start with two non-equilibrated simulation boxes in contact. Each box contains either the C_1 or C_2 FVT–predicted coexistence volume fractions of discotics and depletants. The oblates are arranged in two columnar phases with the same column axes, whereas the depletants are distributed randomly without discotic–depletant overlaps.

The oblates are arranged in two columnar phases with the same column axes, whereas the depletants are distributed randomly without discotic-depletant overlaps. Both boxes contain the same initial number of discotic particles (720) arranged in 16 columns. The two distinct discotic concentration in each simulation box are set via the intra-columnar distance between the discotics along the columnar axes. The initial number of depletants in each of these boxes is set following theoretical predictions. This leads to the number of depletants between 34718 and 13765 in the C_1 phase, and between 7720 and 5340 in the C_2 phase. The whole simulation box contain N particles, with N in between, roughly, 44000 and 20000 particles ($N = N_c = 1440$(OHSCs) + N_d(PHSs), with N_d between 42483 and 19107). A Monte Carlo (MC) cycle is defined as N trials to displace and/or rotate a randomly chosen particle plus an attempt to change the aspect ratio of the simulation box (its volume is fixed).

Two different equilibration steps are considered. Firstly, 1×10^6 cycles are conducted restricting the depletants to the volumes that they occupied in the initial configuration (equilibration of the discotic phases). Secondly, 3×10^6 cycles are carried out without restrictions (equilibration of the direct coexistence). Ensemble-averaged equilibrium discotic

and depletant volume fractions are collected over an additional 2×10^6 cycles. It is noted that in these last two steps the particles can move freely between the simulation boxes and the entire simulation box becomes available for the depletants. The separation between two initial simulation sub-boxes only affects the depletants (a MC move that implies a move of a depletant from one sub-box to the other is rejected) in the first equilibration step. To determine the direct coexistence between two different phases, density profiles of OHSCs and PHSs have been calculated along the side of the simulation box parallel to the columnar axis. To calculate these density profiles, the simulation box was divided in 200 bins along the direction of the columnar axis, averaging the density on these bins along the production run. Figure S4 of the SI shows an example of the density profiles obtained. The density profiles in the simulation box reveal that the discotics and depletants are distributed in two regions with different concentrations of both components. Within the columns the density profiles of the discotics exhibit an oscillatory distribution arrangement. From the average of the density profiles it is possible to calculate the packing fraction of the OHSCs and PHSs in both regions. These direct coexistence simulations were blind-tested: two starting configurations at different colloid packing fractions in the absence of depletants or with a depletant concentration out of the theoretical binodal concentrations merge into a single one.

To characterize the structural properties of the phases at coexistence, equilibrium direct-coexistence MC discotic and depletant volume fractions are used for two independent sets of simulations. These simulations ran for 1×10^6 cycles to equilibrate, plus 2×10^6 cycles for. The number of discotic particles was set to 640, arranged initially in 16 columns. The number of depletants was set according to the geometrical FVT predictions, and range from about 3000 to 75000. The discotic-discotic and discotic-depletant distribution functions. The discotic–discotic and discotic–depletant distribution functions are calculated to elucidate the structural details of the C_1 and C_2 phases. Particularly relevant in our case are the perpendicular and parallel distribution functions, $g(r_\parallel) \equiv g_\parallel$ and $g(r_\perp) \equiv g_\perp$. The perpendicular distribution function $g_\perp$ quantifies the correlation between particles with a given

perpendicular to the nematic director projection of the inter-particle distance, calculated via:

$$g_{\perp}^{i,j} = \frac{N_{\perp}^{i,j}(r_{\perp})}{N_i N_j N_m V_{\perp}/V} \ , \tag{S21}$$

where i and j refer to the species whose correlation is calculated (discotic–discotic, discotic–depletant or depletant–depletant), $r_{\perp}$ is the projection of the distance between two particles in the direction on the direction perpendicular to the nematic director vector. This vector is calculated with the standard methods of diagonalize a traceless tensor $\mathbf{Q}$.[12] $N_{\perp}(r_{\perp})$ is the number of pairs of particles of species i and j that are found at a distance perpendicular to the nematic director between $r_{\perp}$ and $r_{\perp} + \Delta_{\perp}$ in the N_m configurations explored; $\Delta_{\perp}$ is the bin-width used. In our case, we have divided the distance plotted in Figure 3(b,c) of the main text over 200 bins. N_i and N_j are the numbers of particles of species i and j; $V_{\perp}$ is the volume of each bin. In this case, $V_{\perp} = 4\pi/3\{[R^2 - (r_{\perp} + \Delta_{\perp})^2]^{3/2} - (R^2 - r_{\perp}^2)^{3/2}\}$, where V is the total volume of the simulation box (the volume of the system).

To characterize the columnar order, we have employed the discotic–discotic distribution functions in $r_{\parallel}$, $g_{\parallel}^{00}$ (discotics within the same column) and $g_{\parallel}^{01}$ (discotics in adjacent columns), both calculated via the generic expression

$$g_{\parallel}^{lm} = \frac{N_{\parallel}^{lm}(r_{\parallel})}{N_c^2 N_m V_{\parallel}^{lm}/V} \ , \tag{S22}$$

where lm is either 00 or 01. $N_{\parallel}^{00}$ is the number of discotic particles whose inter-particle perpendicular distance is $r_{\perp} < D/2$, and have a parallel distance $r_{\parallel}$ between $r_{\parallel}$ and $r_{\parallel} + \Delta_{\parallel}$ along the N_m configuration explored. For $N_{\parallel}^{01}$ the calculation is the similar, but $r_{\parallel}$ lies in between $D/2$ and $3D/2$. $V_{\parallel}^{lm}$ is the volume of a cylinder with height $\Delta_{\parallel}$ and radius $D/2$ for the 00 case and a cylindrical annulus with internal and external radius $D/2$ and $3D/2$ for the 01 case.

The columnar partition coefficient K_{C} from simulations is approximated as the ratio of

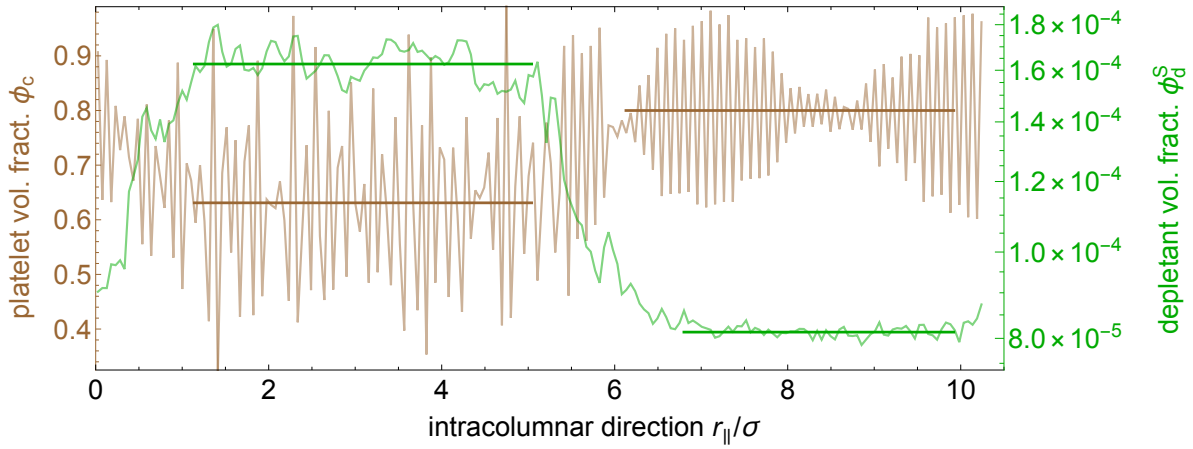

Figure S2: Visualization of how the averaged platelet and depletant volume fractions from the direct coexistence simulation were extracted.

$g_\perp^{\text{c-d}}$ at $r_\perp = 0$ and in the first maximum (at $r_\perp = r_\perp^{\max} \approx D/2 + 4\Delta$):

$$K_C^{\text{sim}} = \frac{g_\perp^{\text{c-d}}(r_\perp = 0)}{g_\perp^{\text{c-d}}(r_\perp = r_\perp^{\max})}, \tag{S23}$$

where $g_\perp^{\text{c-d}} \equiv g_\perp^{\text{discotic–depletant}}$; we use the superscript 'c' for the discotics for simplicity (c might also stand for 'colloid').

In Figure S2, an example of how the final discotic and depletant volume fractions providing the tie-line from Monte Carlo (MC) simulations is presented. Further, in Figure S3, simulation snapshots of the C_1 and C_2 equilibrium phases used in the generation of the distribution functions are shown.

Description of discotic particles

Theoretically, we accounted for platelets as hard cylinders (HCs).[2] In simulations, discotics are modelled as oblate hard spherocylinders (OHSCs).[13] These choices are not fortuitous: theories using HCs are more tractable than with OHSCs,[14,15] whereas the contact detection algorithm implemented in simulations[13] is more efficient for OHSCs than for HCs. Contrary to the HCs, where there are edges present, the OHSC is have surface without edges and

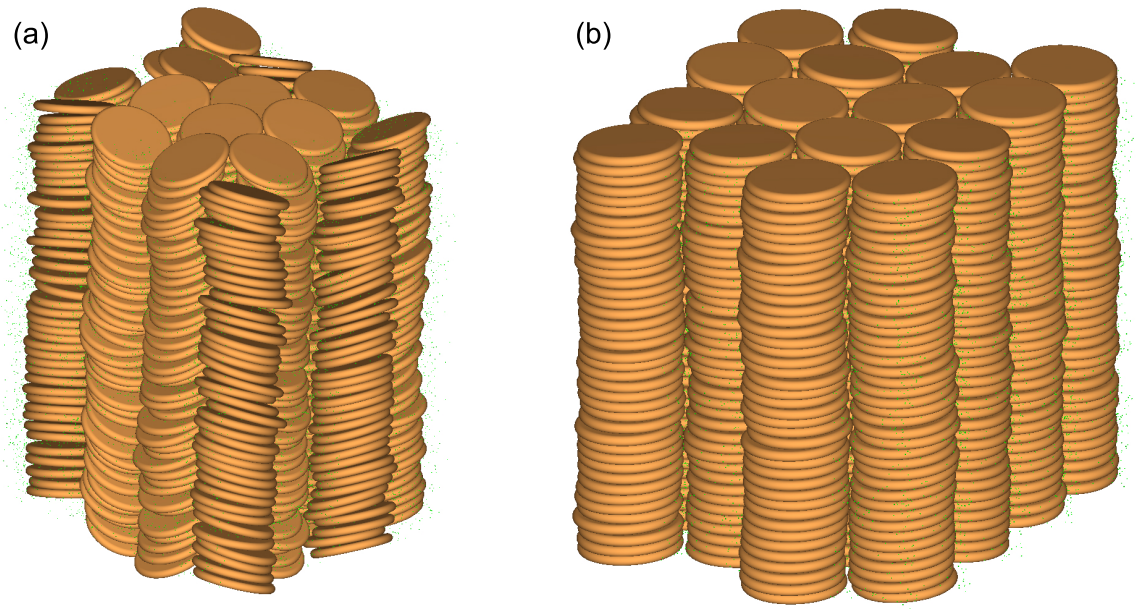

Figure S3: Snapshots of the single-box equilibrium configurations of the C_1(a) and C_2(b) coexisting phases.

hence it is more efficient for simulation purposes.[13] It is convenient to compare results in terms of the absolute relative thickness of the discotics. For the HCs,

$$\Lambda = \frac{L}{D} \, . \tag{S24}$$

The simple transformation

$$\Lambda' = \frac{L}{L+D} = \frac{\Lambda}{1+\Lambda} \tag{S25}$$

allows comparing discotics with the same relative absolute thickness by replacing Λ with Λ' in the HC expressions. The relative size of the penetrable hard sphere (PHS) depletant, which relates to the range of attraction, is defined via the size ratio

$$q = \frac{2\delta}{D} \equiv \frac{2\delta\Lambda}{L} \, , \tag{S26}$$

with δ the PHS diameter and D the HC diameter. For OHSCs with total diameter $D + L$:

$$q' = \frac{q}{1 + \Lambda} \ . \tag{S27}$$

For both discotic mesogens, closed expressions for the excluded volume as a function of the interparticle angle γ (see Figure S4) are available.[14,16] This excluded volume is defined as the volume inaccessible to a second particle in the system as a consequence of the presence of a first particle.[17] The excluded volume between HPs is calculated from:[16]

$$\frac{v_{\text{exc}}^{\text{HC-HC}}}{v_{\text{HC}}} = 2\left(|\cos\gamma| + \frac{4E\left(\sin\gamma\right)}{\pi} + 1\right) + \frac{8\Lambda\sin\gamma}{\pi} + \frac{2\sin\gamma}{\Lambda} \ , \tag{S28}$$

where $E(x)$ is the complete elliptic integral of the second kind. For OHSCs, we follow:[14]

$$\frac{v_{\text{exc}}^{\text{OHSC-OHSC}}}{v_{\text{OHSC}}} = 8 + \frac{12\sin\gamma\left[(\pi^2 - 8)\, y(\Lambda) + \pi\right]}{\pi y(\Lambda)\left[4y(\Lambda)^2 + 3\pi y(\Lambda) + 6\right]} \ , \tag{S29}$$

with

$$y(\Lambda) = \frac{\Lambda}{1 - \Lambda} \ . \tag{S30}$$

In Figure S4 we present the relative excluded volume as a function of the particle orientation γ for two aspect ratios. We note here that we use v_{HC} and v_{OHSC} as the discotic volume v_{c} defined in the main text. It turns out that the minimum excluded volume configuration is retained for particles aligned about their axes of symmetry:

$$v_{\text{exc}}|_{\gamma=0} = v_{\text{exc}}|_{\gamma=\pi} = 8v_{\text{p}} \ ,$$

and corresponds to the hard-sphere equivalent excluded volume: four times the particle volume per particle (thus 8 as the excluded volume is for a pair of particles). This configuration corresponds to particle pairs aligned along their flat faces, which in a columnar phase corre-

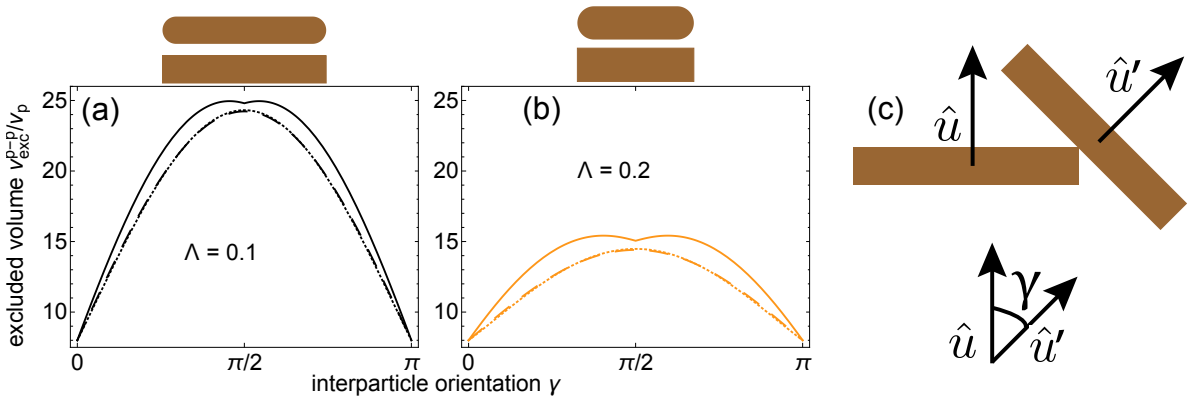

Figure S4: (a,b) Excluded volume between hard cylinders (solid curves) and excluded volume between hard oblate spherocylinders (OHSCs) with $\Lambda \equiv L/D = 0.1$ (a) and $\Lambda = 0.2$ (b) as indicated. The dashed and dotted curves correspond to the OHSC–OHSC excluded volume as given by Piastra[14] and by Mulder.[15] (c) Schematic representation of particle orientations, given by the vectors $\hat{u}$ and $\hat{u}'$, and therefore by the single inter-particle orientation angle γ.

sponds to the intra-columnar direction $r_{\parallel}$. The maximum excluded volume for OHSCs pairs occurs exactly at $\gamma = \pi/2$ while for HPs the maximum excluded volume exhibits two shallow symmetric maxima around $\gamma = \pi/2$.

Phase diagram of depletant-free platelet suspensions

Various thermodynamic properties of hard cylinders (HCs) have been previously studied in detail.[1,18] For the isotropic and nematic phases we apply Onsager–Parsons-Lee theory.[1,19] The resulting free energy of both the isotropic and nematic phases reads:

$$\frac{\widetilde{F}_k}{\phi_c} = \ln \widetilde{v}_c + \ln \phi_c - 1 + \sigma_k[f(\hat{u})] + \frac{2}{\pi}\frac{\phi_c}{\Lambda} G_P \langle\langle \Theta_k^{Exc}(\hat{u}, \hat{u}')\rangle\rangle \ . \tag{S31}$$

The first two terms on the right-hand-side of Equation S31 correspond to the finite-volume normalization of the energy ($\widetilde{v}_c$ being the dimensionless thermal volume of a platelet) and the ideal gas contribution to the free energy.

In order to calculate the free energy using Equation S31, an orientational distribution function [ODF, $f(\hat{u})$] is needed. A system in which particle orientations are taken into

account can be envisaged as a multi-component system in which each component corresponds to a possible particle orientation.[16,20] Hence, the ODF is a measure of the probability of finding a particle with a given orientation $\hat{u}$ [see Figure S4(c)]. The rotational entropy term, $\sigma_k[f(\hat{u})]$ is defined as:[19]

$$\sigma_k[f(\hat{u})] = \int f(\hat{u}) \ln[4\pi f(\hat{u})] \mathrm{d}\hat{u} \ . \tag{S32}$$

The dimensionless ensemble-averaged excluded volume follows from:

$$\langle\langle \Theta_k^{\mathrm{Exc}}(\hat{u}, \hat{u}')\rangle\rangle = \frac{1}{D^3} \int\int f(\hat{u}) f(\hat{u}') v_{\mathrm{exc}}^{\text{HC-HC}}(\hat{u} \cdot \hat{u}') \mathrm{d}\hat{u}\, \mathrm{d}\hat{u}' \ . \tag{S33}$$

Entropy-driven phase transitions[21] depend on the excluded volume between two discotic particles. We use Equation S28 to quantify the excluded volume between HCs. Finally, effects beyond the second osmotic virial coefficient are accounted for in an approximate manner via the Parsons-Lee scaling factor:[22,23]

$$G_{\mathrm{P}} = \frac{4 - 3\phi_{\mathrm{c}}}{4(1 - \phi_{\mathrm{c}})^2} \ . \tag{S34}$$

Formally, at each platelet concentration the free energy of the system must be minimized with respect to the ODF, $f(\hat{u})$. Analytical expressions for the ODF can be obtained for the isotropic state by considering equiprobability of orientations: $f(\hat{u}) = 1/(4\pi)$. Hence, $\sigma_{\mathrm{I}}[f(\hat{u})] = 0$, and by applying the so-called isotropic averages ($\langle\langle \sin\gamma \rangle\rangle_{\mathrm{I}} = \pi/4$, $\langle\langle E\{\sin\gamma\}\rangle\rangle_{\mathrm{I}} = \pi^2/8$, and $\langle\langle \cos\gamma \rangle\rangle_{\mathrm{I}} = 1/2$). Consequently, the free energy of an isotropic ensemble of HCs can be written as:[1]

$$\frac{\widetilde{F}_{\mathrm{I}}}{\phi_{\mathrm{c}}} = \ln \widetilde{v}_{\mathrm{c}} + \ln \phi_{\mathrm{c}} - 1 + \frac{2}{\pi} \frac{\phi_{\mathrm{c}}}{\Lambda} G_{\mathrm{P}} \Theta_{\mathrm{I}}^{\mathrm{Exc}} \ , \tag{S35}$$

with:

$$\Theta_{\mathrm{I}}^{\mathrm{Exc}} = \frac{\pi^2}{8} + \left(\frac{3\pi}{4} + \frac{\pi^2}{4}\right)\Lambda + \frac{\pi\Lambda^2}{2} \ . \tag{S36}$$

Furthermore, closed expressions for the free energy of the nematic phase can be obtained via a Gaussian approximation[24] for $f(\hat{u})$. Considering that all relative orientations can be defined as a Gaussian perturbation from the nematic director vector provides a closed-form expression for the free energy.[1] This Gaussian ODF reads

$$f_{\mathrm{N}}(\theta) = \frac{\kappa}{4\pi}\exp\left[-\frac{1}{2}\kappa\theta^2\right] \ , \tag{S37}$$

where θ is the polar angle between the nematic director and the orientation of the platelet. Minimizing the free energy with respect to the unknown parameter of the Gaussian ODF κ provides a closed form for the free energy of the nematic phase:[1]

$$\frac{\widetilde{F}_{\mathrm{N}}}{\phi_{\mathrm{c}}} = \ln\widetilde{v}_{\mathrm{c}} + \ln\phi_{\mathrm{c}} - 1 + \sigma_{\mathrm{N}} + \frac{2}{\pi}\frac{\phi_{\mathrm{c}}}{\Lambda}G_{\mathrm{P}}\Theta_{\mathrm{N}}^{\mathrm{Exc}} \ , \tag{S38}$$

with:

$$\sigma_{\mathrm{N}} = \ln\left[\frac{\pi\phi_{\mathrm{c}}^2 G_{\mathrm{P}}^2}{4\Lambda^2}\right] - 1 \ ,$$

and

$$\Theta_{\mathrm{N}}^{\mathrm{Exc}} = \frac{1}{2}\pi^{3/2}\kappa(\phi_{\mathrm{c}},\Lambda)^{-1/2} + 2\pi\Lambda \ .$$

We note here that we follow an approximate, perturbative approach for the ODF instead of a full self-consistent numerical optimization.[25–27] The latter approach is exact but would slow down the computations of the phase diagrams of discotic-depletant mixtures tremendously, therefore hampering the calculation of, for example, four-phase co-existences. Moreover,

given the high discotic volume fractions, we do not expect large deviations between the Gaussian-based nematic free energy and the full-numerical solution. The Gaussian approximation is accurate for sharply peaked ODF's, which occur actually in case of depletion-mediated attractions. See for instance Eur. Phys. J. E 23, 355–365 (2007) for a comparison of using the Gaussian ODF as compared to the numerical ODF. Another advantage of the Gaussian PDF is that algebraic expressions can be obtained for the free energy expressions.

For the columnar phase, a modified Lennard-Jones-Devonshire (LJD) cell-theory[28] provides a closed expression for the free energy.[1,29] We add a constant term $(-\ln 4)$ to the original expressions[1,29] such that the nematic–columnar phase coexistence is closer to the one reported via computer simulations:[1,30]

$$\begin{aligned}\frac{\widetilde{F}_{\mathrm{C}}}{\phi_{\mathrm{c}}} &= \ln\widetilde{v}_{\mathrm{c}} + \ln\phi_{\mathrm{c}} - 3 - 2\ln\left[1-\frac{1}{\widehat{\Delta}_{\perp}}\right] \\ &\quad + 2\ln\left[\frac{3\widehat{\Delta}_{\perp}^{2}\widetilde{\phi}_{\mathrm{c}}}{2\Lambda\left(1-\widehat{\Delta}_{\perp}^{2}\widetilde{\phi}_{\mathrm{c}}\right)}\right] - \ln\left[\frac{1}{3}\left(1-\widehat{\Delta}_{\perp}^{2}\widetilde{\phi}_{\mathrm{c}}\right)\right] - \ln 4\ ,\end{aligned} \tag{S39}$$

with the lateral spacing (inter-columnar direction):

$$\widehat{\Delta}_{\perp} \equiv \Delta_{\perp}/\sigma = \frac{\sqrt[3]{2}\bar{K}^{2/3} - \sqrt[3]{34}\widetilde{\phi}_{\mathrm{c}}}{6^{2/3}\sqrt[3]{\bar{K}}\widetilde{\phi}_{\mathrm{c}}}\ , \tag{S40}$$

where

$$\bar{K} = \sqrt{3(\widetilde{\phi}_{\mathrm{c}})^{3}(243\widetilde{\phi}_{\mathrm{c}}+32)} + 27\widetilde{\phi}_{\mathrm{c}}^{2}\ , \tag{S41}$$

and with

$$\widetilde{\phi}_{\mathrm{c}} = \phi_{\mathrm{c}}/\phi_{\mathrm{c}}^{\mathrm{cp}}\ , \tag{S42}$$

and

$$\phi_{\rm c}^{\rm cp} = \pi/(2\sqrt{3}) \approx 0.907 \ . \tag{S43}$$

An approximate expression for the intra-columnar spacing[29] $\Delta_\parallel$ is:

$$\widehat{\Delta}_\parallel \equiv \Delta_\parallel/L = \frac{1}{\phi_{\rm c}^{\rm r}\widehat{\Delta}_\perp^2} \ . \tag{S44}$$

From the free energy expressions, standard thermodynamic relations enable to resolve resolve the (dimensionless) chemical potential of the discs and osmotic pressure of the dispersion for a given k-phase ($k = \{\mathrm{I}, \mathrm{N}, \mathrm{C}\}$):

$$\beta\mu_k^{\rm o} \equiv \widetilde{\mu}_k^{\rm o} = \left(\frac{\partial \widetilde{F}_k}{\partial \phi_{\rm c}}\right)_{T,V} \ ; \ \beta\Pi_k^{\rm o} v_{\rm c} \equiv \widetilde{\Pi}_k^{\rm o} = \phi_{\rm c}\widetilde{\mu} - \widetilde{F}_k \ . \tag{S45}$$

Equilibrium coexisting phases follow from the condition of equal chemical potential and osmotic pressure:

$$\widetilde{\mu}_i^{\rm o} = \widetilde{\mu}_j^{\rm o}, \text{ and } \widetilde{\Pi}_i^{\rm o} = \widetilde{\Pi}_j^{\rm o} \ , \tag{S46}$$

which allow to compute I–N, I–C, and N–C phase coexistence at a given Λ. This can be easily extended to calculate the three phase coexistence:

$$\widetilde{\mu}_{\rm I}^{\rm o} = \widetilde{\mu}_{\rm N}^{\rm o} = \widetilde{\mu}_{\rm C}^{\rm o} \ , \text{ and } \widetilde{\Pi}_{\rm I}^{\rm o} = \widetilde{\Pi}_{\rm N}^{\rm o} = \widetilde{\Pi}_{\rm C}^{\rm o} \ . \tag{S47}$$

The superscript 'o' is used to denote the (depletant-free) chemical potential and osmotic pressure in dispersions of discs. The theoretically obtained phase diagram obtained is compared with simulation results in Figure S5. As observed, the phase boundaries from theory and simulations are in remarkably close agreement.

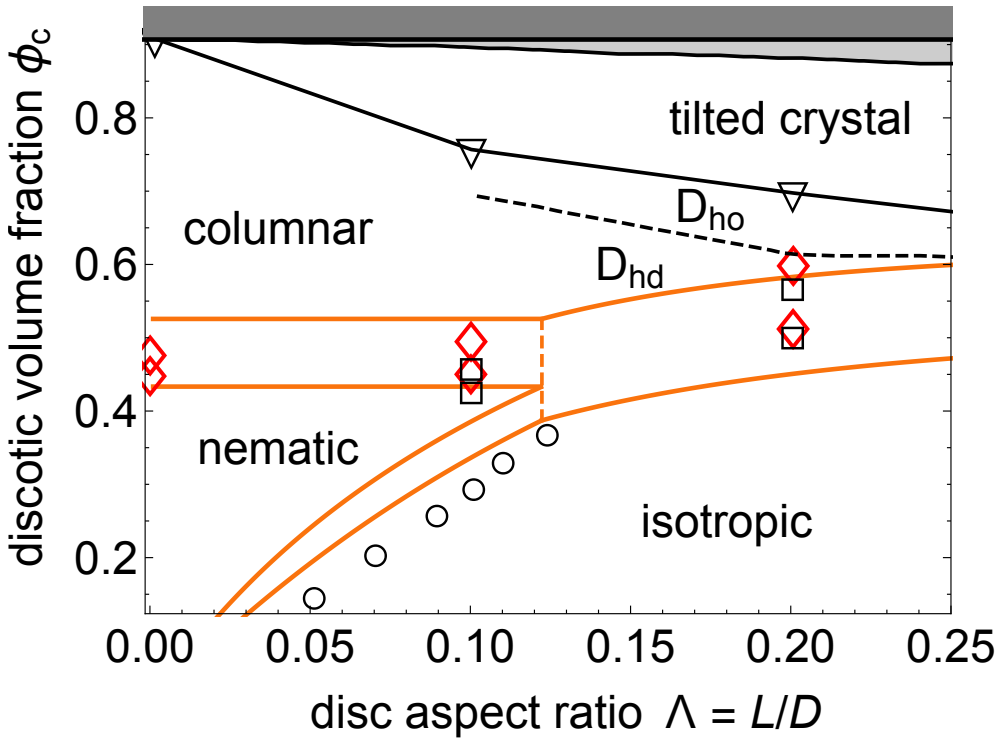

Figure S5: Theoretical phase diagram of a pure platelet suspension in the $\{\Lambda, \phi_c\}$ phase-space. Dark gray area corresponds to the forbidden region for hard cylinders (volume fractions above close packing). Simulation results from Marechal *et al.*[13] for oblate hard spherocylinders are presented in black: circles correspond to the isotropic–nematic phase transition, squares indicated the nematic–columnar, and triangles hold for the transition from columnar to tilted crystal. In simulations, a difference has been made between two columnar phases: D_{hd} (discotic disordered) and D_{ho} (discotic ordered). The term (dis)ordered points towards the discotic–discotic correlantion in the intra-columnar direction.

Phase diagram scan and compartmentalisation: further theoretical predictions

In Figures S6 to S9 theoretically-predicted phase diagrams for illustrative Λ- and q-values are presented, along with a scan in the number of depletants in the intra- and inter-columnar directions. On the top panels, complete phase diagrams as that in Figure 3(a) of the main text are presented. In the middle panel, the free volume fraction for depletants is shown as in Figure 2 of the main text; the inset corresponds to ratio of α_C^{simp} over the complete expression. In the bottom panels, we focus on the C_1–C_2 coexistence; as can be appreciated

the depletant concentration that follows from the weighted arithmetic mean considering the two directional αs is always close to the binodal calculated using the complete expression.

We now turn our attention to the N–(C_1C_1) critical endpoint (CEP) for which FVT predictions are plotted in Figure S10 for $\Lambda = 0.1$ and $q = 0.01$. To find the CEP (orange diamond) at a fixed Λ, one might simply scan the triple point associated to the C_1–C_2 coexistence, and check at which q-value the triple point (TP, purple curves) and the critical point (CP, orange curve) coincide [Figure S10(a)]. As observed for HSs mixed with PHSs at low q,[4] ϕ_c at the C_1–C_2 critical point ($\phi_c^{\parallel}$) decreases with increasing q. The N–C_1–C_2 CEP occurs at $q \approx 0.04$, significantly above the original prediction ($q \approx 0.02$).[2] The maximum strength of the depletion between two discs $W_{\mathrm{AOV}}^{\mathrm{max}}$,

$$\frac{W_{\mathrm{AOV}}^{\mathrm{max}}}{k_{\mathrm{B}}T} = -\phi_{\mathrm{d}}^{\mathrm{R}} \left(\frac{3}{4q^2} + \frac{3\pi}{8q} + 1 \right) \ , \tag{S48}$$

at the triple points is presented in Figure S10(b). As the depletant concentration at the I–N–C_2 coexistence (grey curve) is always above the one of the N–C_1–C_2 (see inset), the same holds for the depletion attraction strength [Equation S48]. This attraction strength decays exponentially at the N–C_1–C_2 triple point. Also in line with what is observed for HSs mixed with tiny PHSs,[4] the $\phi_{\mathrm{d}}^{\mathrm{R}}$-value at the N–$C_1$–$C_2$ triple point first increases and then decreases with increasing q. This denotes a soft re-entrant behavior.[31] The C_1–C_2 critical point occurs at a depletant concentration which is virtually zero for all q: the mere presence of depletants in the system is enough to induce two different columnar states due to the directionality of the pockets available for depletants in the system. While not reported previously for model colloidal systems (as far as we are aware of), such behavior of the critical point is quite common in alloys.[32]

In Figure S11 a collection triple point(TP) curves is presented at fixed Λ with increasing q both below and above the depletant-free three phase coexistence, which provide the CEP values indicated with discs in Figure S12(a) (diamonds in Figure S11).

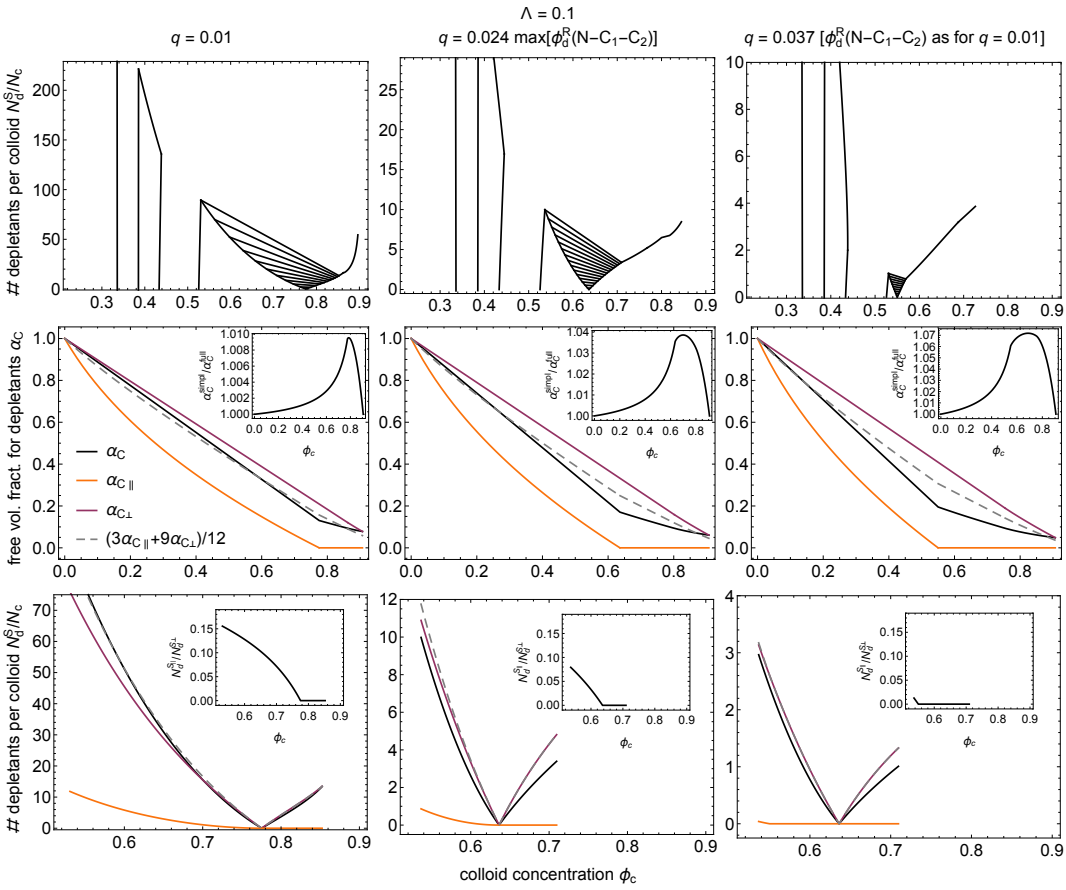

Figure S6: Top panels: phase diagrams in the discotic volume fraction–number of depletants per discotic phase space with increasing relative depletant size q at fixed platelet aspect ratio $\Lambda = 0.1$; black lines are example C_1-C_2 tie-lines. Middle panels: free volume fraction for depletants in the columnar phase; (I) complete expression α_C (black curves); (II) small-system in the intra-columnar direction $\alpha_{C\parallel}$ (orange curves); (III) small-system in the inter-columnar direction $\alpha_{C\perp}$ (purple curves); (IV) the weighted-average of $\alpha_{C\parallel}$ and $\alpha_{C\perp}$ indicated (dashed, grey curves). Insets are the ratio of the free-volume fraction without considering the edges of the platelet α_C^{simp} to α_C. Bottom panels: phase diagrams generated with the α-expressions considered (same color code as middle panels). Insets show the partition coefficient of depletants in the intra- and inter-columnar directions along the C_1-C_2 binodal.

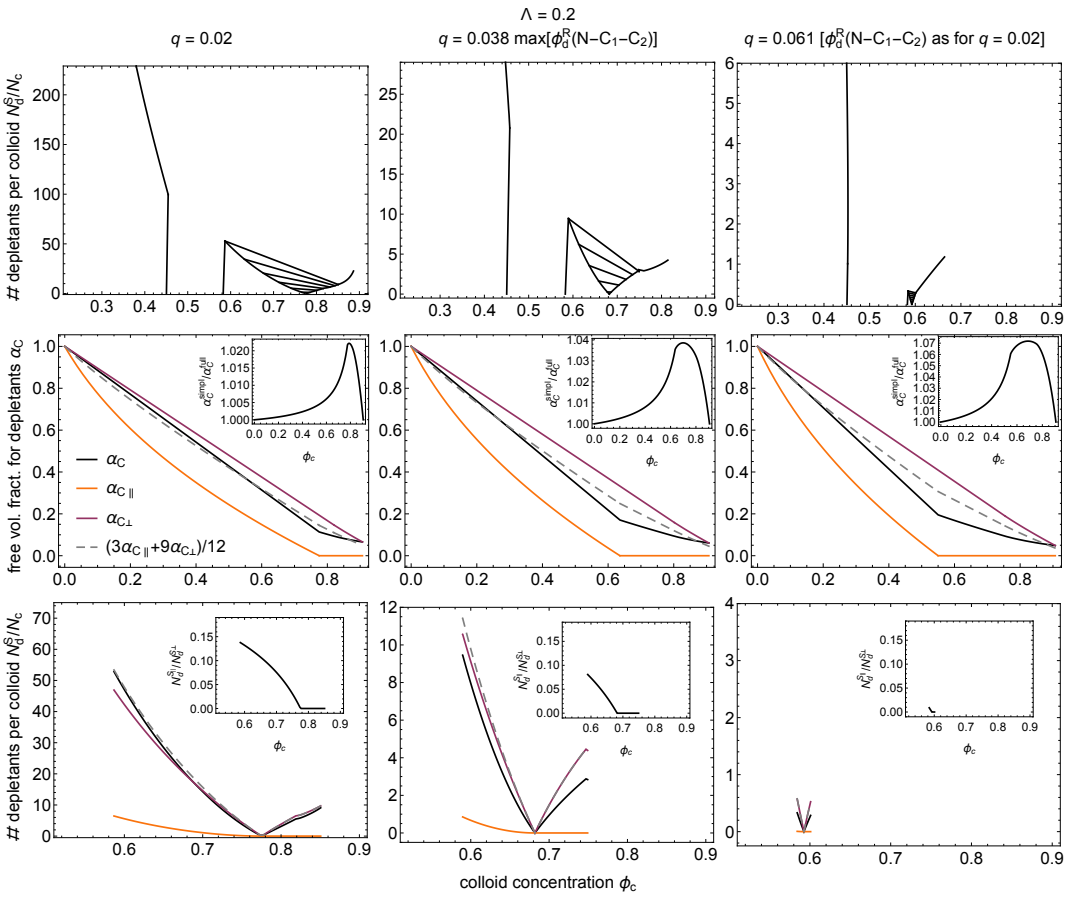

Figure S7: Similar to Figure S6, but for $\Lambda = 0.2$ and the q-values indicated.

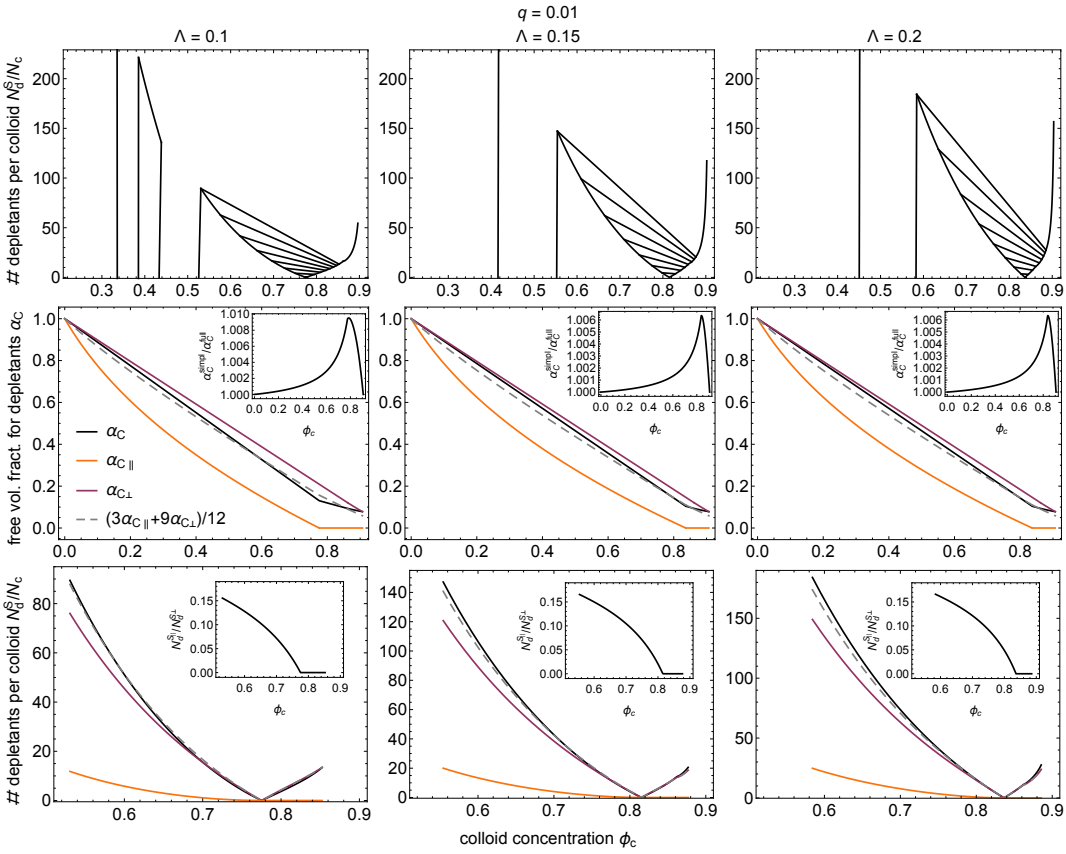

Figure S8: Similar to Figure S6, but for variable Λ and fixed $q = 0.01$ as indicated.

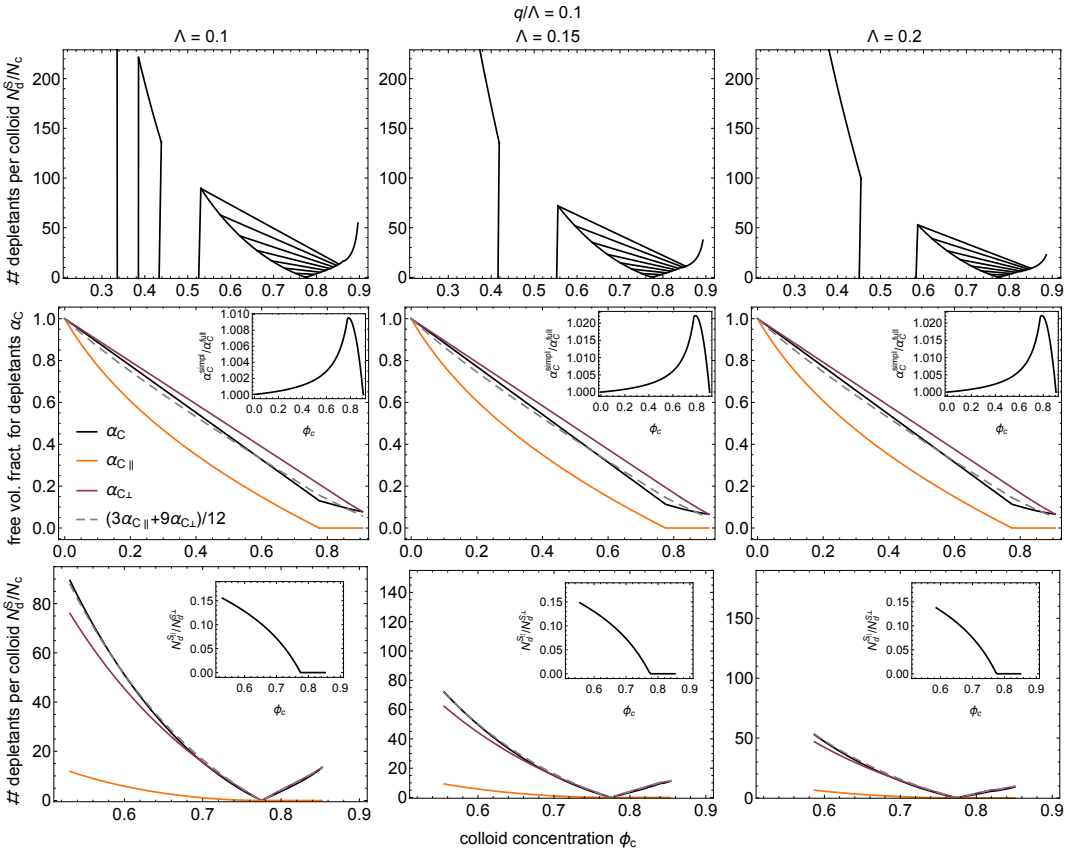

Figure S9: Similar to Figure S6, but for fixed $q/\Lambda = 0.1$.

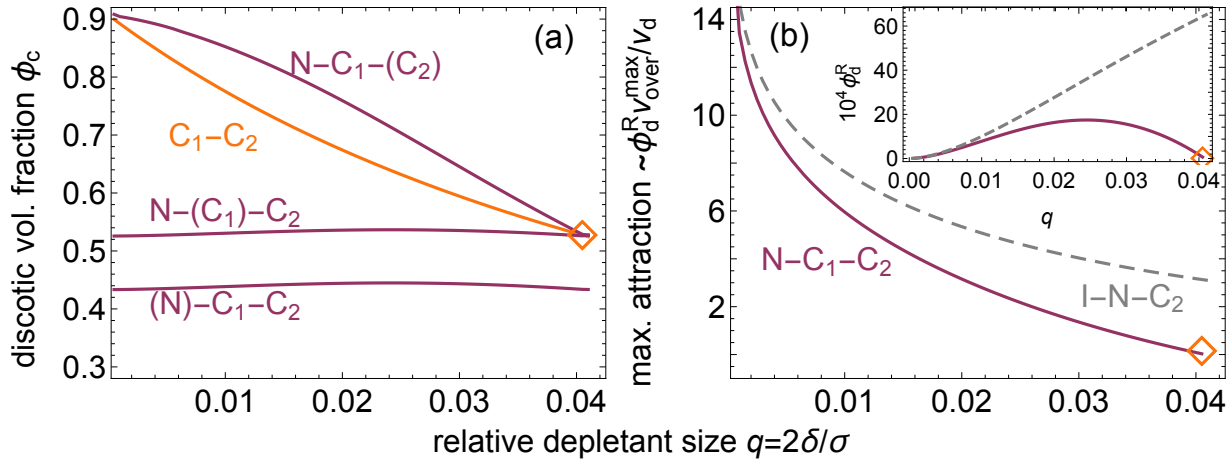

Figure S10: (a) Discotic volume fraction (ϕ_c) at the nematic–columnar–columnar (N–C_1–C_2) triple point (purple curves) and at the columnar–columnar (C_1–C_2) critical point (orange curve) as a function of the relative depletant size q. For the three phase coexistence, the parenthesis denotes the phase referred to. (b) Maximum strength of the depletion attraction at N–C_1–C_2 (purple curve) and at the I–N–C_2 triple points (dashed grey curve) as a function of the relative depletant size q . In the inset, the depletant concentration in the reservoir ϕ_d^R is shown. The open orange symbols denote the critical endpoint.

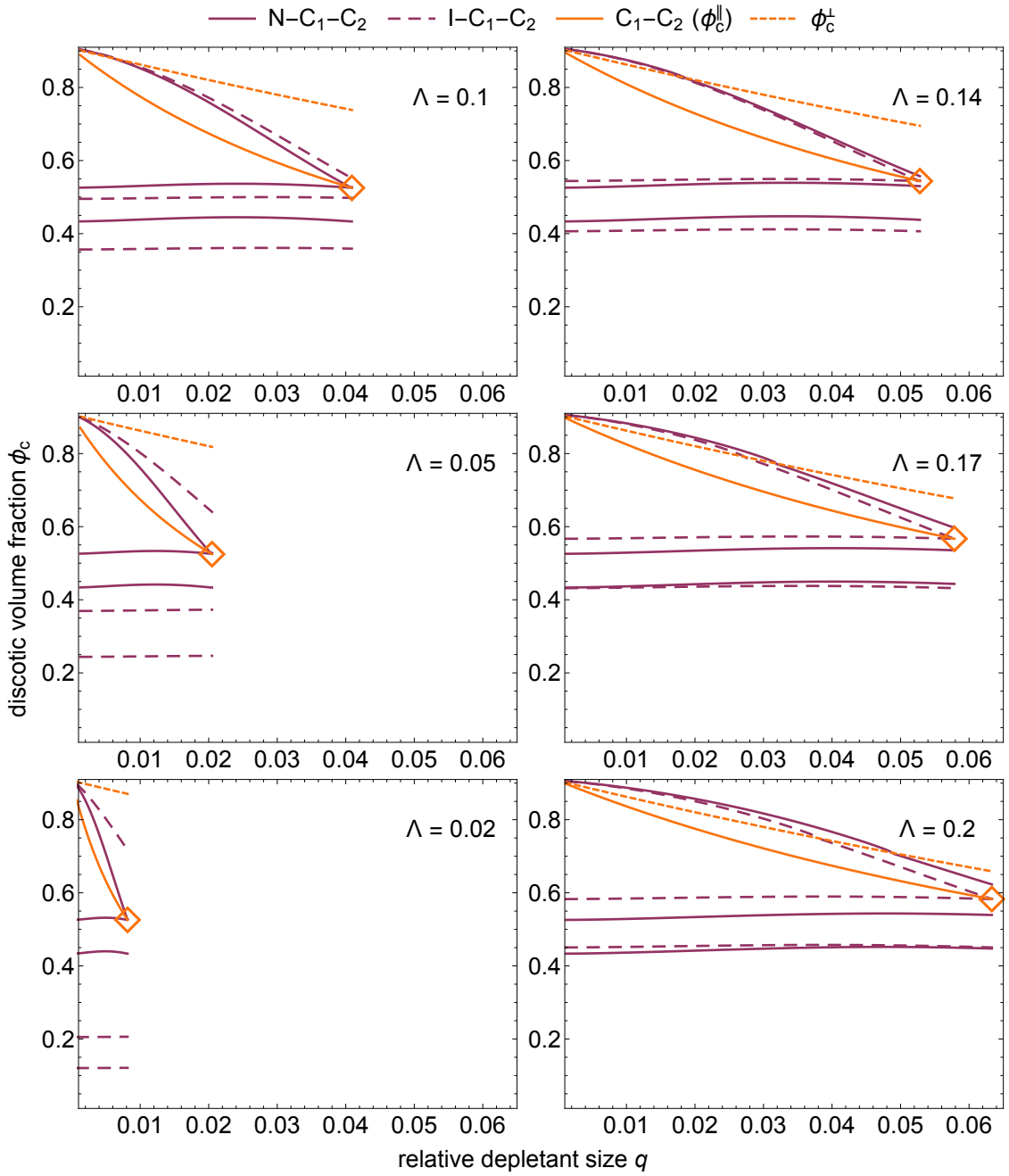

Figure S11: Discotic volume fractions at the N–C_1–C_2 triple point (solid purple curves), at the I–C_1–C_2 triple point (dashed purple curves), at the C_1–C_2 critical point (solid orange curve), and at the point from which overlap in the inter-columnar direction occurs ($\phi_c^{\perp}$) as a function of the relative depletant size q. Discotic aspect ratio Λ as indicated. The critical end point is indicated with an orange rhombus.

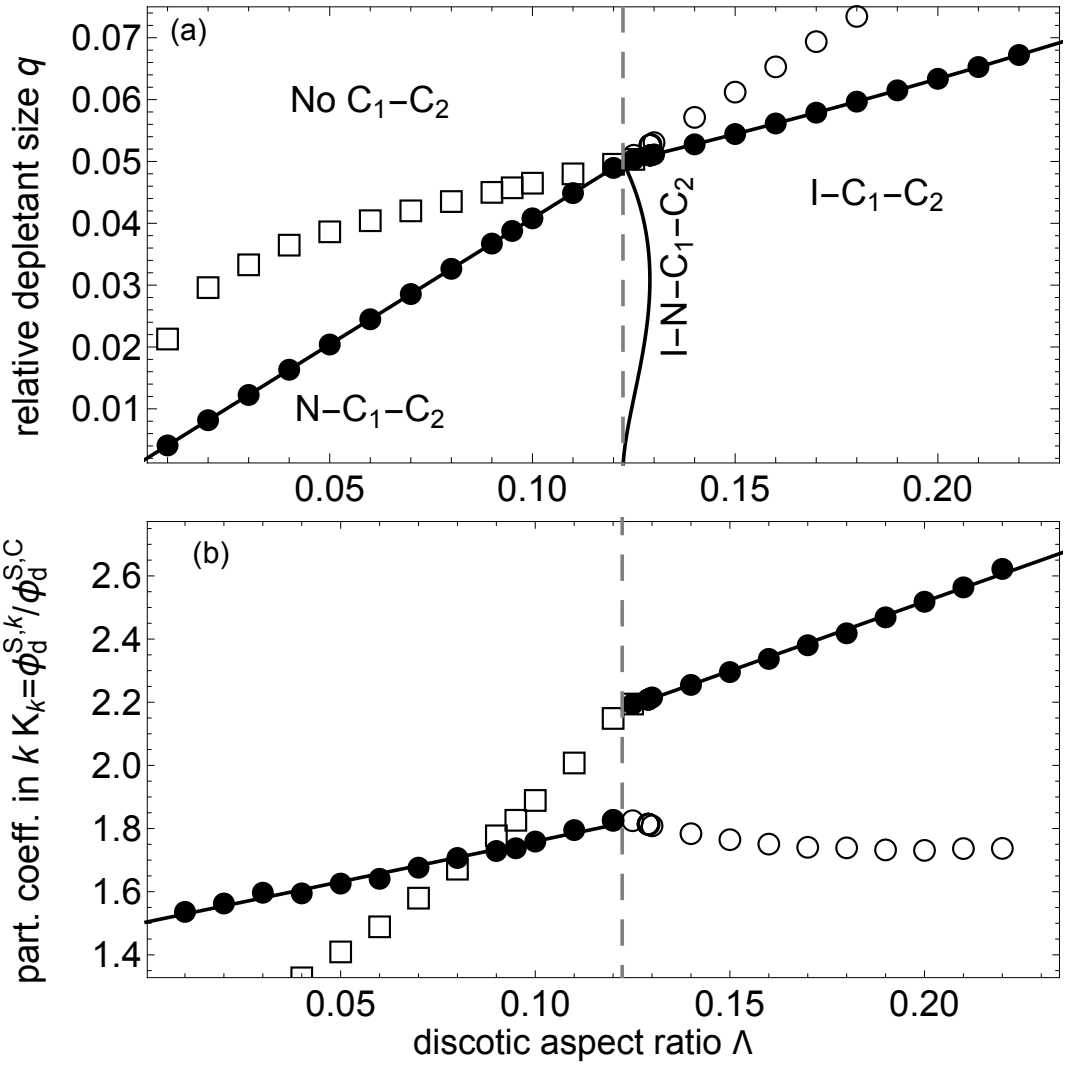

Figure S12: (a) Similar to Figure 6 of main text, but showing the data used to calculate the CEP curves (discs). Circles and squares correspond to the metastable NCC (circles) and ICC (squares) CEP curves. (b) Partition coefficient of depletants at the CEP of the N–(C_1C_1) and at the CP of the I–(C_1C_1). Metastable CEPs follow the same symbol-code as in (a).

References

(1) Wensink, H. H.; Lekkerkerker, H. N. W. Phase diagram of hard colloidal platelets: a theoretical account. *Mol. Phys.* **2009**, *107*, 2111–2118.

(2) González García, Á.; Tuinier, R.; Maring, J. V.; Opdam, J.; Wensink, H. H.; Lekkerkerker, H. N. W. Depletion-driven four-phase coexistences in discotic systems. *Molecular Physics* **2018**, *116*, 2757–2772.

(3) Lekkerkerker, H. N. W. Osmotic equilibrium treatment of the phase separation in colloidal dispersions containing non-adsorbing polymer molecules. *Colloids Surf.* **1990**, *51*, 419–426.

(4) González García, Á.; Opdam, J.; Tuinier, R.; Vis, M. Isostructural solid–solid coexistence of colloid–polymer mixtures. *Chemical Physics Letters* **2018**, *709*, 16 – 20.

(5) Tejero, C. F.; Daanoun, A.; Lekkerkerker, H. N. W.; Baus, M. Phase diagrams of "simple" fluids with extreme pair potentials. *Phys. Rev. Lett.* **1994**, *73*, 752–755.

(6) Tuinier, R.; Fleer, G. J. Critical endpoint and analytical phase diagram of attractive hard-core Yukawa spheres. *J. Phys. Chem. B* **2006**, *110*, 20540–20545.

(7) Lekkerkerker, H. N. W.; Poon, W. C. K.; Pusey, P. N.; Stroobants, A.; Warren, P. B. Phase Behaviour of Colloid + Polymer Mixtures. *Europhys. Lett.* **1992**, *20*, 559.

(8) Widom, B. Some Topics in the Theory of Fluids. *J. Chem. Phys.* **1963**, *39*, 2808.

(9) Helfand, E.; Reiss, H.; Frisch, H. L.; Lebowitz, J. L. Scaled Particle Theory of Fluids. *J. Chem. Phys.* **1960**, *33*, 1379–1385.

(10) Lebowitz, J. L.; Helfand, E.; Praestgaard, E. Scaled Particle Theory of Fluid Mixtures. *J. Chem. Phys.* **1965**, *43*, 774–779.

(11) Cuetos, A.; Martínez-Haya, B. Columnar phases of discotic spherocylinders. *The Journal of Chemical Physics* **2008**, *129*, 214706.

(12) Allen, M. P.; Evans, G. T.; Frenkel, D.; Mulder, B. M. *Advances in Chemical Physics*; John Wiley & Sons, Ltd, 2007; pp 1–166.

(13) Marechal, M.; Cuetos, A.; Martínez-Haya, B.; Dijkstra, M. Phase behavior of hard colloidal platelets using free energy calculations. *J. Chem. Phys.* **2011**, *134*, 094501.

(14) Piastra, M.; Virga, E. G. Onsagerian formula for the excluded volume of spherodisks. *Phys. Rev. E* **2013**, *88*, 064501.

(15) Mulder, B. M. The excluded volume of hard sphero-zonotopes. *Molecular Physics* **2005**, *103*, 1411–1424.

(16) Onsager, L. The effects of shape on the interaction of colloidal particles. *Ann. N. Y. Acad. Sci.* **1949**, *51*, 627–659.

(17) Baus, M.; Tejero, C. F. *Equilibrium Statistical Physics*, 1st ed.; Springer, Berlin, Heidelberg, 2008.

(18) van Anders, G.; Klotsa, D.; Ahmed, N. K.; Engel, M.; Glotzer, S. C. Understanding shape entropy through local dense packing. *Proc. Natl. Acad. Sci. U.S.A.* **2014**, *111*, E4812–E4821.

(19) Wensink, H. H.; Vroege, G. J.; Lekkerkerker, H. N. W. Isotropic'Nematic Density Inversion in a Binary Mixture of Thin and Thick Hard Platelets. *J. Phys. Chem B* **2001**, *105*, 10610–10618.

(20) van Roij, R. The isotropic and nematic liquid crystal phase of colloidal rods. *Eur. J. Phys.* **2005**, *26*, S57.

(21) Dijkstra, M. In *Advances in Chemical Physics*; Rice, S. A., Dinner, A. R., Eds.; John Wiley & Sons, Inc., 2014; Vol. 156; Chapter 2.

(22) Parsons, J. D. Nematic ordering in a system of rods. *Phys. Rev. A* **1979**, *19*, 1225–1230.

(23) Lee, S.-D. A numerical investigation of nematic ordering based on a simple hard?rod model. *J. Chem. Phys.* **1987**, *87*, 4972–4974.

(24) Odijk, T. Theory of lyotropic polymer liquid crystals. *Macromolecules* **1986**, *19*, 2313–2329.

(25) Lekkerkerker, H. N. W.; Tuinier, R. *Colloids and the Depletion Interaction*; Springer, Heidelberg, 2011.

(26) Dabat, T.; Hubert, F.; Paineau, E.; Launois, P.; Laforest, C.; Grégoire, B.; Dazas, B.; Tertre, E.; Delville, A.; Ferrage, E. A general orientation distribution function for clay-rich media. *Nat. Commun. 10*, 5456.

(27) Skutnik, R. A.; Lehmann, L.; Püschel-Schlotthauer, S.; Jackson, G.; Schoen, M. The formation of biaxial nematic phases in binary mixtures of thermotropic liquid-crystals composed of uniaxial molecules. *Mol. Phys. 117*, 2830–2845.

(28) Lennard-Jones, J. E.; Devonshire, A. F. Critical Phenomena in Gases. I. *Proc. R. Soc A* **1937**, *163*, 53–70.

(29) Wensink, H. H. Equation of State of a Dense Columnar Liquid Crystal. *Phys. Rev. Lett.* **2004**, *93*, 157801.

(30) Veerman, J. A. C.; Frenkel, D. Phase behavior of disklike hard-core mesogens. *Phys. Rev. A* **1992**, *45*, 5632–5648.

(31) Foffi, G.; McCullagh, G. D.; Lawlor, A.; Zaccarelli, E.; Dawson, K. A.; Sciortino, F.; Tartaglia, P.; Pini, D.; Stell, G. Phase equilibria and glass transition in colloidal systems with short-ranged attractive interactions: Application to protein crystallization. *Phys. Rev. E* **2002**, *65*, 031407.

(32) Fernandes, C.; Senos, A. Cemented carbide phase diagrams: A review. *Int. J. Refract. Met. Hard Mater.* **2011**, *29*, 405 – 418.